We are IntechOpen, the world's leading publisher of Open Access books
Built by scientists, for scientists

4,800
Open access books available

122,000
International authors and editors

135M
Downloads

Our authors are among the

154
Countries delivered to

TOP 1%
most cited scientists

12.2%
Contributors from top 500 universities

CLARIVATE ANALYTICS
BOOK CITATION INDEX
INDEXED

WEB OF SCIENCE™

Selection of our books indexed in the Book Citation Index in Web of Science™ Core Collection (BKCI)

Interested in publishing with us?
Contact book.department@intechopen.com

Numbers displayed above are based on latest data collected.
For more information visit www.intechopen.com

9

Self-Landmarking for Robotics Applications

Yanfei Liu and Carlos Pomalaza-Ráez
Indiana University – Purdue University Fort Wayne
USA

1. Introduction

This chapter discusses the use of self-landmarking with autonomous mobile robots. Of particular interest are outdoor applications where a group of robots can only rely on themselves for purposes of self-localization and camera calibration, e.g. planetary exploration missions. Recently we have proposed a method of active self-landmarking which takes full advantage of the technology that is expected to be available in current and future autonomous robots, e.g. cameras, wireless transceivers, and inertial navigation systems (Liu, & Pomalaza-Ráez, 2010a).

Mobile robots' navigation in an unknown workspace can be divided into the following tasks; obstacle avoidance, path planning, map building and self-localization. Self-localization is a problem which refers to the estimation of a robot's current position. It is important to investigate technologies that can work in a variety of indoor and outdoor scenarios and that do not necessarily rely on a network of satellites or a fixed infrastructure of wireless access points. In this chapter we present and discuss the use of active self-landmarking for the case of a network of mobile robots. These robots have radio transceivers for communicating with each other and with a control node. They also have cameras and, at the minimum, a conventional inertial navigation system based on accelerometers, gyroscopes, etc. We present a methodology by which robots can use the landmarking information in conjunction with the navigation information, and in some cases, the strength of the signals of the wireless links to achieve high accuracy camera calibration tasks. Once a camera is properly calibrated, conventional image registration and image based techniques can be used to address the self-localization problem.

The fast calibration model described in this chapter shares some characteristics with the model described in (Zhang, 2004) where closed-form solutions are presented for a method that uses 1D objects. In (Zhang, 2004) numerous (hundreds) observations of a 1D object are used to compute the camera calibration parameters. The 1D object is a set of 3 collinear well defined points. The distances between the points are known. The observations are taken while one of the end points remains fixed as the 1D object moves. Whereas this method is proven to work well in a well structured scenario it has several disadvantages it is to be used in an unstructured outdoors scenario. Depending on the nature of the outdoor scenario, e.g. planetary exploration, having a moving long 1D object might not be cost effective or even feasible. The method described in this chapter uses a network of mobile robots that can communicate with each other and can be implemented in a variety of outdoor environments.

2. Landmarks

Humans and animals use several mechanisms to navigate space. The nature of these mechanisms depends on the particular navigational problem. In general, global and local landmarks are needed for successful navigation (Vlasak, 2006; Steck & Mallot, 2000). As their biological counterparts, robots use landmarks that can be recognized by their sensory systems. Landmarks can be natural or artificial and they are carefully chosen to be easy to identify. Natural landmarks are those objects or features that are already in the environment and their nature is independent of the presence or not of a robotic application, e.g. a building, a rock formation. Artificial landmarks are specially designed objects that are placed in the environment with the objective of enabling robot navigation.

2.1 Natural landmarks

Natural landmarks are selected from some salient regions in the scene. The processing of natural landmarks is usually a difficult computational task. The main problem when using natural landmarks is to efficiently detect and match the features present in the sensed data. The most common type of sensor being used is a camera-based system. Within indoor environments, landmark extraction has been focused on well defined objects or features, e.g. doors, windows (Hayet et al., 2006). Whereas these methods have provided good results within indoor scenarios their application to unstructured outdoor environments is complicated by the presence of time varying illumination conditions as well as dynamic objects present in the images. The difficulty of this problem is further increased when there is little or no *a priori* knowledge of the environment e.g., planetary exploration missions.

2.2 Artificial landmarks

Artificial landmarks are manmade, fixed at certain locations, and of certain pattern, such as circular (Lin & Tummala, 1997; Zitova & Flusser, 1999), patterns with barcodes (Briggs et al., 2000), or colour pattern with symmetric and repetitive arrangement of colour patches (Yoon & Kweon, 2001). Compared with natural landmarks, artificial landmarks usually are simpler; provide a more reliable performance; and work very well for indoor navigation. Unfortunately artificial landmarks are not an option for many outdoor navigation applications due to the complexity and expansiveness of the fields that robots traverse. Since the size and shape of the artificial landmarks are known in advance their detection and matching is simpler than when using natural landmarks. Assuming that the position of the landmarks is known to a robot, once a landmark is recognized, the robot can use that information to calculate its own position.

3. Camera calibration

Camera calibration is the process of finding: (a) the internal parameters of a camera such as the position of the image centre in the image, the focal length, scaling factors for the row pixels and column pixels; and (b) the external parameters such as the position and orientation of the camera. These parameters are used to model the camera in a reference system called world coordinate system.

The setup of the world coordinate system depends on the actual system. In computer vision applications involving industrial robotic systems (Liu et al., 2000), a world coordinate

system for the robot is often used since the robot is mounted on a fixed location. For autonomous mobile robotic network, there are two ways to incorporate a vision system. One is to have a distributed camera network located in fixed locations (Hoover & Olsen, 2000; Yokoya et al., 2008). The other one is to have the camera system mounted on the robots (Atiya & Hager, 2000). Either of these two methods has its own advantages and disadvantages. The fixed camera network can provide accurate and consistent visual information since the cameras don't move at all. However, it has constraints on the size of the area being analysed. Also even for a small area at least four cameras are needed to form a map for the whole area. The camera-on-board configurations do not have limitations on how large the area needs to be and therefore are suited for outdoor navigation.

The calibration task for a distributed camera network in a large area is challenging because they must be calibrated in a unified coordinate system. In (Yokoya et al., 2008), a group of mobile robots with one robot equipped with visual marker were developed to conduct the calibration. The robot with the marker was used as the calibration target. So as long as the cameras are mounted in fixed locations a fixed world coordinate system can be used to model the camera. However, for mobile autonomous robot systems with cameras on board, a still world coordinate system is difficult to find especially for outdoor navigation tasks due to the constantly changing robots' workspace. Instead the camera coordinate system, i.e. a coordinate system on the robot, is chosen as the world coordinate system. In such case the external parameters are known. Hence the calibration process in this chapter only focuses on the internal parameters.

The standard calibration process has two steps. First, a list of 3D world coordinates and their corresponding 2D image coordinates is established. Second, a set of equations using these correspondences is solved to model the camera. A target with certain pattern, such as grid, is often constructed and used to establish the correspondences (Tsai, 1987). There is a large body of work on camera calibration techniques developed by the photogrammetry community as well as by computer vision researchers. Most of the techniques assume that the calibration process takes place on a very structured environment, i.e. laboratory setup, and rely on well defined 2D (Tsai, 1987) or 3D calibration objects (Liu et al., 2000). The use of 1D objects (Zhang, 2004; Wu et al., 2005) as well as self calibration techniques (Faugeras, 2000) usually come at the price of an increase in the computation complexity. The method introduced in this chapter has low numerical complexity and thus its computation is relatively fast even when implemented in simple camera on-board processors.

3.1 Camera calibration model

The camera calibration model discussed in this section includes the mathematical equations to solve for the parameters and the method to establish a list of correspondences using a group of mobile robots. We use the camera pinhole model that was first introduced by the Chinese philosopher Mo-Di (470 BCE to 390 BCE), founder of Mohism (Needham, 1986).

In a traditional camera, a lens is used to bend light waves into a narrow beam that produces an image on the film. With a pinhole camera, the hole acts like a lens by only allowing a narrow beam of light to enter. The pinhole camera produces the same type of upside-down, reversed image as a modern camera, but with significantly fewer parts.

3.1.1 Notation

For the pinhole camera model (Fig. 1) a 2D point is denoted as $\boldsymbol{a_i} = [a_{ix} \quad a_{iy}]^T$. A 3D point is denoted as $\boldsymbol{A_i} = [A_{ix} \quad A_{iy} \quad A_{iz}]^T$. In Fig. 1 $\boldsymbol{p} = [p_y \quad p_y]^T$ is the point where the principal

axis intersects the image plane. Note that the origin of the image coordinate system is in the corner. f is the focal length.

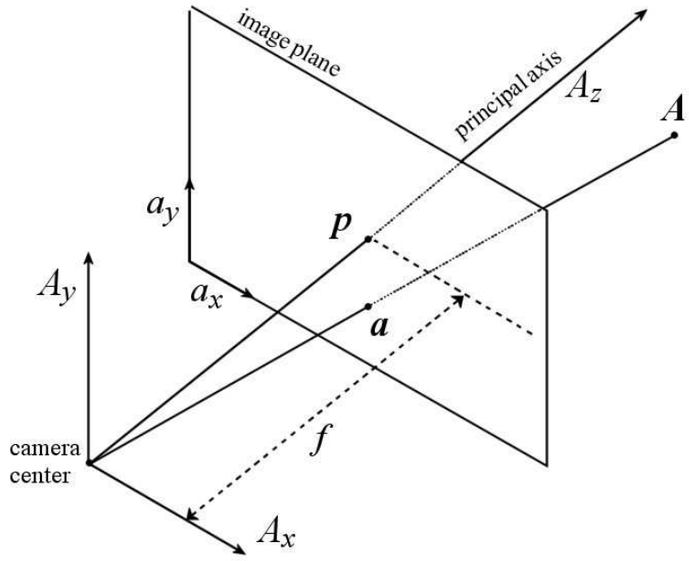

Fig. 1. Normalized camera coordinate system.

The augmented vector $\tilde{a}_i$ is defined as $\tilde{\boldsymbol{a}}_{\boldsymbol{i}} = [a_{ix} \quad a_{iy} \quad 1]^T$. In the same manner $\tilde{\boldsymbol{A}}_{\boldsymbol{i}}$ is defined as $\tilde{\boldsymbol{A}}_{\boldsymbol{i}} = [A_{ix} \quad A_{iy} \quad A_{iz} \quad 1]^T$. The relationship between the 3D point $\boldsymbol{A}_{\boldsymbol{i}}$ and its projection $\boldsymbol{a}_{\boldsymbol{i}}$ is given by,

$$z_{\boldsymbol{A}_i}\tilde{\boldsymbol{a}}_i = \boldsymbol{K}[\boldsymbol{R} \quad \boldsymbol{t}]\tilde{\boldsymbol{A}}_i \tag{1}$$

where $\boldsymbol{K}$ stands for the camera intrinsic matrix,

$$\boldsymbol{K} = \begin{bmatrix} \alpha & \gamma & u_0 \\ 0 & \beta & v_0 \\ 0 & 0 & 1 \end{bmatrix} \tag{2}$$

and

$$\boldsymbol{K}^{-1} = \begin{bmatrix} \frac{1}{\alpha} & -\frac{\gamma}{\alpha\beta} & \frac{\gamma v_0 - u_0\beta}{\alpha\beta} \\ 0 & \frac{1}{\beta} & -\frac{v_0}{\beta} \\ 0 & 0 & 1 \end{bmatrix} \tag{3}$$

$[u_0 \quad v_0]$ are the coordinates of the principal point in pixels, α and β are the scale factors for the image u and v axes, and γ stands for the skew of the two image axes. $[\boldsymbol{R} \quad \boldsymbol{t}]$ stands for the extrinsic parameters and it represents the rotation and translation that relates the world coordinate system to the camera coordinate system. In our case, the camera coordinate system is assumed to be the world coordinate system, $\boldsymbol{R} = \boldsymbol{I}$ and $\boldsymbol{t} = \boldsymbol{0}$.
If $\gamma = 0$ as it is the case for CCD and CMOS cameras then,

$$\boldsymbol{K} = \begin{bmatrix} \alpha & 0 & u_0 \\ 0 & \beta & v_0 \\ 0 & 0 & 1 \end{bmatrix} \tag{4}$$

and

$$\boldsymbol{K}^{-1} = \begin{bmatrix} \frac{1}{\alpha} & 0 & -\frac{u_0}{\alpha} \\ 0 & \frac{1}{\beta} & -\frac{v_0}{\beta} \\ 0 & 0 & 1 \end{bmatrix} \tag{5}$$

The K matrix can also be written as,

$$\boldsymbol{K} = \begin{bmatrix} m_x f & 0 & m_x p_x \\ 0 & m_y f & m_y p_y \\ 0 & 0 & 1 \end{bmatrix} \tag{6}$$

Where m_x, m_y are the number of pixels per meter in the horizontal and vertical directions. It should be mentioned that CMOS based cameras can be implemented with fewer components, use less power, and/or provide faster readout than CCDs. CMOS sensors are also less expensive to manufacture than CCD sensors.

3.1.2 Mathematical model

The model described in this section is illustrated in Fig. 2. The reference camera is at position $\boldsymbol{R_i}$ while the landmark is located at position $\boldsymbol{A_i}$.

The projection of the landmark in the image plane of the reference camera changes when the camera moves from position 0 to position 1 as illustrated in Fig. 2.

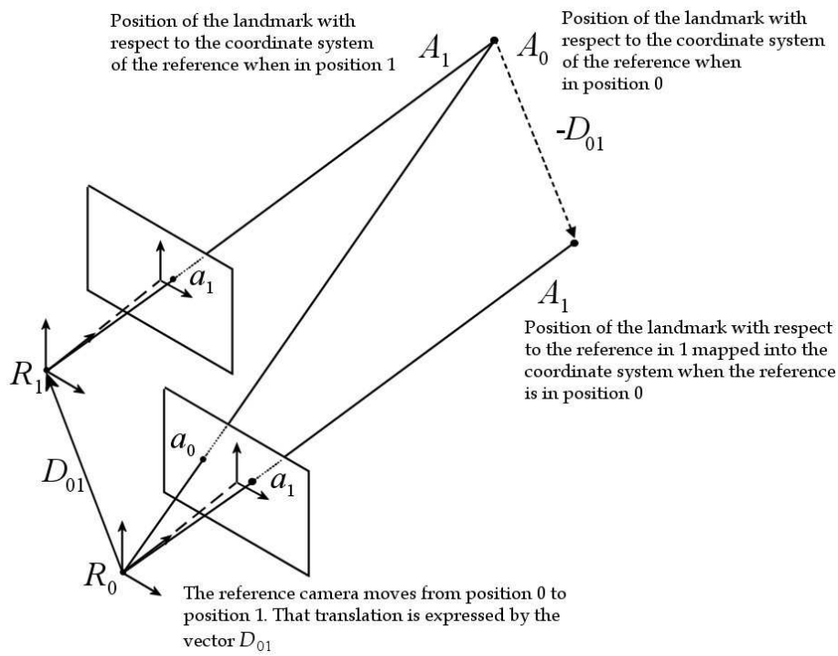

Fig. 2. Changes in the image coordinates when the reference camera or the landmark moves.

This motion is represented by the vector $\boldsymbol{D_{01}}$. If instead the landmark moves according to $-D_{01}$, as shown in Fig. 2, and the reference camera does not move, then both the location of the landmark, $\boldsymbol{A_1}$, and its projection on the image, $\boldsymbol{a_1}$, would be the same as in the case when the reference camera moves.

For any location of the landmark, $\boldsymbol{A_i}$, and its projection on the image, $\boldsymbol{a_i}$.

If $\tilde{\boldsymbol{a}}_{\boldsymbol{i}} = \begin{bmatrix} a_{ix} & a_{iy} & 1 \end{bmatrix}^T$ with $\boldsymbol{R} = \boldsymbol{I}$ and $\boldsymbol{t} = \boldsymbol{0}$ from eq. (1), then

$$\boldsymbol{A}_i = z_{\boldsymbol{A}_i} \boldsymbol{K}^{-1} \tilde{\boldsymbol{a}}_i \tag{7}$$

also define

$$\boldsymbol{D}_{ij} = \boldsymbol{A}_j - \boldsymbol{A}_i = \begin{bmatrix} d_{ijx} & d_{ijy} & d_{ijz} \end{bmatrix}^T \tag{8}$$

The magnitudes of $\boldsymbol{A}_i, \boldsymbol{A}_j$, and $\boldsymbol{D}_{ij}$ (L_{A_i}, L_{A_j}, and $L_{D_{ij}}$, respectively) can be estimated using the strength of the received signal. Also for D_{ij} it is possible to estimate $L_{D_{ij}}$ using the data from the robot navigational systems. Both estimation methods, signal strength on a wireless link and navigational system data, have certain amount of error that should be taken into account in the overall estimation process.

$$L_{\boldsymbol{A}_j}^2 = \boldsymbol{A}_j{}^T \boldsymbol{A}_j = \left(\boldsymbol{A}_i{}^T + \boldsymbol{D}_{ij}{}^T\right)\left(\boldsymbol{A}_i + \boldsymbol{D}_{ij}\right)$$

$$= \boldsymbol{A}_i{}^T \boldsymbol{A}_i + \boldsymbol{A}_i{}^T \boldsymbol{D}_{ij} + \boldsymbol{D}_{ij}{}^T \boldsymbol{A}_i + \boldsymbol{D}_{ij}{}^T \boldsymbol{D}_{ij} \tag{9}$$

$$L_{\boldsymbol{A}_j}^2 = L_{\boldsymbol{A}_i}^2 + L_{\boldsymbol{D}_{ij}}^2 + 2\boldsymbol{D}_{ij}{}^T \boldsymbol{A}_i \tag{10}$$

$$\boldsymbol{D}_{ij}{}^T \boldsymbol{A}_i = \frac{L_{\boldsymbol{A}_j}^2 - L_{\boldsymbol{A}_i}^2 - L_{\boldsymbol{D}_{ij}}^2}{2}$$

$$= \boldsymbol{D}_{ij}{}^T z_{\boldsymbol{A}_i} \begin{bmatrix} \frac{1}{\alpha} & 0 & -\frac{u_0}{\alpha} \\ 0 & \frac{1}{\beta} & -\frac{v_0}{\beta} \\ 0 & 0 & 1 \end{bmatrix} \begin{bmatrix} a_{ix} \\ a_{iy} \\ 1 \end{bmatrix} \tag{11}$$

Define δ_{ij} as,

$$\delta_{ij} = \frac{L_{\boldsymbol{A}_j}^2 - L_{\boldsymbol{A}_i}^2 - L_{\boldsymbol{D}_{ij}}^2}{2} =$$

$$= z_{\boldsymbol{A}_i} \begin{bmatrix} d_{ijx} & d_{ijy} & d_{ijz} \end{bmatrix} \begin{bmatrix} M_1 & 0 & M_2 \\ 0 & M_3 & M_4 \\ 0 & 0 & 1 \end{bmatrix} \begin{bmatrix} a_{ix} \\ a_{iy} \\ 1 \end{bmatrix} \tag{12}$$

where,

$$M_1 = \frac{1}{\alpha} \quad M_2 = -\frac{u_0}{\alpha} \quad M_3 = \frac{1}{\beta} \quad M_4 = -\frac{v_0}{\beta} \tag{13}$$

for $0 \le i < j \le N$

Where N is the number of locations where the landmark moves to

$$\delta_{ij} = z_{\boldsymbol{A}_i} \left[a_{ix} d_{ijx} M_1 + d_{ijx} M_2 + a_{iy} d_{ijy} M_3 + d_{ijy} M_4 + d_{ijz} \right] \tag{14}$$

At the end of this section it is shown that $z_{\boldsymbol{A}_i}$ can be separately estimated from the values of the M_i parameters. Assuming then that $z_{\boldsymbol{A}_i}$ has been estimated,

$$\frac{\delta_{ij}}{z_{\boldsymbol{A}_i}} - d_{ijz} = \begin{bmatrix} a_{ix}d_{ijx} & d_{ijx} & a_{iy}d_{ijy} & d_{ijy} \end{bmatrix} \begin{bmatrix} M_1 \\ M_2 \\ M_3 \\ M_4 \end{bmatrix} \tag{15}$$

Let's define λ_{ij} as,

$$\lambda_{ij} = \frac{\delta_{ij}}{z_{\boldsymbol{A}_i}} - d_{ijz} \tag{16}$$

for $0 \leq i < j \leq N$
Then,

$$\lambda_{ij} = \boldsymbol{c}_{ij}^T \boldsymbol{x} \tag{17}$$

where $\boldsymbol{c_{ij}} = \begin{bmatrix} a_{ix}d_{ijx} & d_{ijx} & a_{iy}d_{ijy} & d_{ijy} \end{bmatrix}^T$ and $\boldsymbol{x} = [M_1 \ M_2 \ M_3 \ M_4 \ ]^T$
If the landmark moves to N locations, $\boldsymbol{A_1}, \boldsymbol{A_2}, \cdots, \boldsymbol{A_N}$, the corresponding equations can be written as,

$$\boldsymbol{\Lambda} = \mathbf{C}\boldsymbol{x} \tag{18}$$

where $\boldsymbol{\Lambda} = \begin{bmatrix} \lambda_{12} & \lambda_{13} & \cdots & \lambda_{1N} & \lambda_{23} & \cdots & \lambda_{(N-1)N} \end{bmatrix}^T$
and $\mathbf{C} = \begin{bmatrix} c_{12} & c_{13} & \cdots & c_{1N} & c_{23} & \cdots & c_{(N-1)N} \end{bmatrix}^T$
The N locations are cross-listed to generate a number of $N(N-1)/2$ pair of points (as shown in Fig. 3) in the equations.

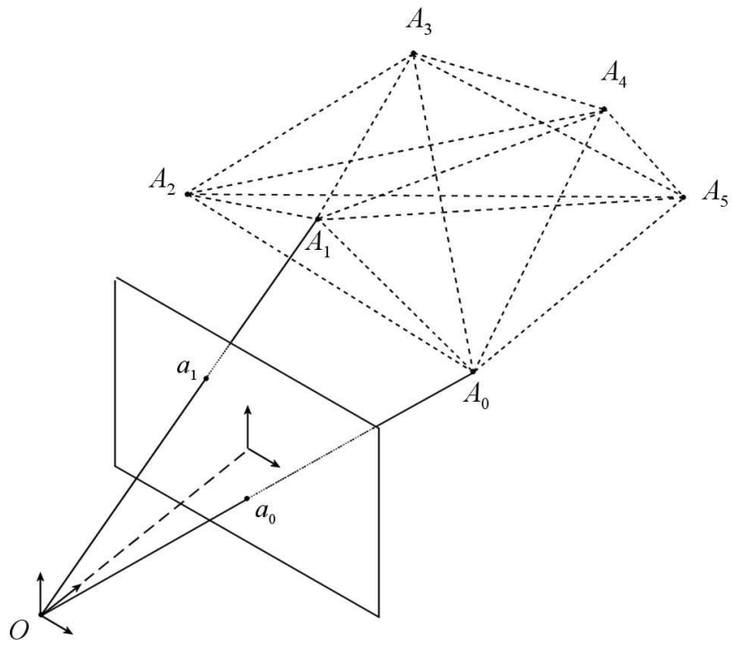

Fig. 3. Cross-listed locations.

The least-squares solution for x is,

$$\boldsymbol{x} = [\mathbf{C}^T\mathbf{C}]^{-1}\mathbf{C}^T\boldsymbol{\Lambda} \tag{19}$$

Once x is estimated the camera intrinsic parameters can be easily computed. Next we will describe two ways to compute z_{A_i}. $A_{iz} = z_{A_i}$, is the projection of the vector A_i on the z-axis. Also $z_{A_i} = z_{A_0} + S_i$ where,

$$S_i = \sum_{j=1}^{i} \delta_{(j-1)jz} \quad \text{for} \quad 1 \le i \le N \tag{20}$$

Thus one way to compute z_{A_i} is to first estimate z_{A_0} and then to use the robot navigation system to obtain the values of $\delta_{(j-1)jz}$ (the displacement along the z-axis as the robot moves) to compute S_i in equation (20). The value of z_{A_0} itself can be using the navigation system as the robot takes the first measurement position.

A second way to compute z_{A_i} relying only on the distance measurement is as follows. From equation (12),

$$\delta_{ij} = z_{\boldsymbol{A_i}}\begin{bmatrix} d_{ijx} & d_{ijy} & d_{ijz} \end{bmatrix}\begin{bmatrix} M_1 a_{ix} + M_2 \\ M_3 a_{iy} + M_4 \\ 1 \end{bmatrix} \tag{21}$$

$$\delta_{ij} = \begin{bmatrix} d_{ijx} & d_{ijy} & d_{ijz} \end{bmatrix}\begin{bmatrix} z_{A_i}(M_1 a_{ix} + M_2) \\ z_{A_i}(M_3 a_{iy} + M_4) \\ z_{A_i} \end{bmatrix} = \boldsymbol{c}_{ij}^T\boldsymbol{x} \tag{22}$$

As the landmark moves to N locations $\boldsymbol{A_1}, \boldsymbol{A_2}, \cdots, \boldsymbol{A_N}$, the corresponding equations can be written as

$$\boldsymbol{\Delta} = \mathbf{C}\boldsymbol{x} \tag{23}$$

where

$$\boldsymbol{\Delta} = [\delta_{i1} \quad \delta_{i2} \quad \delta_{ij} \quad \ldots \quad \delta_{iN}]^T \quad \text{for } j \neq i \tag{24}$$

and

$$\mathbf{C} = [\boldsymbol{c}_{\mathrm{i}1} \ \boldsymbol{c}_{i2} \ \cdots \ \boldsymbol{c}_{iN}]^T \quad \text{for } j \neq i \tag{25}$$

The least-squares solution for x is,

$$\boldsymbol{x} = [\mathbf{C}^T\mathbf{C}]^{-1}\mathbf{C}^T\boldsymbol{\Delta}$$

Once x is estimated, $z_{\boldsymbol{A_i}}$ is also estimated.

4. Self-landmarking

Our system utilizes the paradigm where a group of mobile robots equipped with sensors measure their positions relative to one another. This paradigm can be used to directly address the self-localization problem as it is done in (Kurazume et al., 1996). In this chapter we use self-landmarking as the underlying framework to develop and implement the fast camera calibration procedure described in the previous section. In our case a network of mobile robots travel together as illustrated in Fig. 4. It is assumed that the robots have

cameras and are equipped with radio transceivers that allow for communications among them and with a control node.

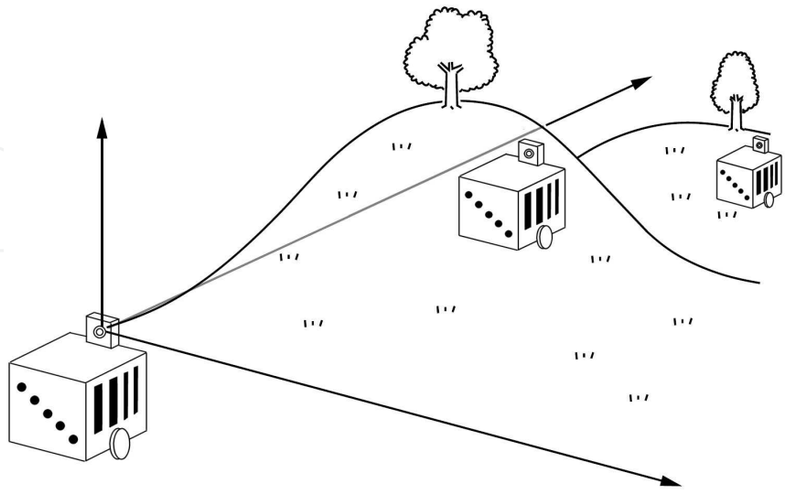

Fig. 4. Self-landmarking mobile robots.

Having decided on using the robots themselves as landmarks to each other the next step is to choose the type of artificial landmark that can be mounted on a robot's body. One possible choice is to use passive landmarks with invariant features such as circular shapes (Zitova & Flusser, 1999) or with simple patterns (Briggs et al., 2000) that are quickly recognizable under a variety of viewing conditions. Whereas these methods have provided good results within indoor scenarios their application to unstructured outdoor environments is complicated by the presence of time varying illumination conditions as well as dynamic objects present in the images. To overcome these drawbacks we have proposed the use of active landmarks.

The current state of LED technology allows for low-power and relative high luminance from these devices. Depending on the constraints imposed by the robot's shape and dimensions one or more LEDs can be located on its outer surface. Since the robots have communication capabilities they can schedule when the LEDs can be turned on and off to match the periods when the cameras are capturing images for image differencing. Power can thus be saved by having the LEDs ON intervals as short as possible. Short ON intervals can also greatly simplify the detection and estimation of the landmarks (the LEDs) in the images since it minimizes the effects of time varying illumination conditions and the motion of other objects in the scene.

Further savings in power can be achieved by using smart cameras. These cameras feature camera-on-a-chip integration (Rinner et al., 2008). For distributed sensing applications this feature allows the cameras to perform a fair amount of on-chip image processing before the information is sent to a central node, e.g. through a wireless channel. For applications where the communications' bandwidth is limited the image processing and data fusion operations carried out on the cameras need to be fast and efficient (Rinner & Wolf, 2008). For our work the detection and location estimation of the landmarks can be reduced to the analysis of a binary image that is obtained by thresholding the difference of the images just before the landmark is turned on and then when it is on. A blob finding algorithm (Liu & Pomalaza-

Ráez, 2010b) can be applied to the task of detecting the landmark. This algorithm is very efficient, i.e. low-complexity, and can be performed on the camera processor. The on-camera chip only needs to report the location (pixel coordinates) of the blob.

5. Wireless localization

Measurements of the strength of the received radio signals can be used to estimate the distance between a transmitter and a receiver. The received signal strength indicator (RSSI) is a measurement that is readily available even in the simple transceivers used in a variety of wireless sensor networks (WSNs). Another common measurement is the link quality indicator (LQI). Both RSSI and LQI can be used for localization by correlating them with distance values. However most of the methods using those estimates have relative large errors in particular within indoor environments (Luthy et al., 2007; Whitehouse et al., 2005).
By combining signal time-of-flight and phase measurements and making use of the full ISM (Industrial, Scientific, Medical) spectrum band it is possible to have estimation errors of less than 20 cm with standard deviations less than 3 cm when using IEEE 802.15.4 devices (Schwarzer et al., 2008). This latter method requires the addition of a low-cost hardware/software that is not part of the 802.15.4 standard. Likewise for IEEE 802.11 devices it is possible, with an extra hardware, to achieve distance estimation measurements with errors less than one meter (Bahillo et al., 2009). The consensus of most researchers is that it is very difficult to guarantee distance estimation errors of less than 10 cm when using 802.11 (Wi-Fi) or 802.15.4 (ZigBee) devices in both indoor and outdoor environments that have many feature rich objects.
Communication systems using Ultra-wide Bandwidth (UWB) signals have shown excellent accuracy in terms of distance measurements (Shimuzi & Sanada, 2003). Using time of arrival (ToA) methods several researchers have reported estimation errors of less than 5 cm in a variety of outdoor and indoor environments (Falsi et al., 2006). UWB signals have been proposed for the detection of vegetation, which can be very useful for outdoor navigation (Liang et al., 2008), and of people behind walls (Zetik et al., 2006) which can be useful in rescue missions. It is then expected that in many applications mobile robots will be equipped with UWB transceivers. It should be noted that the accuracy of common GPS devices is usually more than 10 meters. The Wide Area Augmentation System (WAAS) developed by the Federal Aviation Administration uses a network of GPS reference receivers to increase the accuracy to around 1 meter.

6. Experimental validation

The paradigm described in this chapter is suitable for a wireless mobile robotic network. In principle, the distance from a landmark to a reference camera can be estimated using the wireless communication transceiver that each robot is equipped with. Depending on the type of transceiver, the error in this estimation can be in the order of meters, e.g. for the IEEE 805.15.4 protocol, or in centimeters, e.g. when using UWB technology. Errors in the order of meters are not acceptable for any camera calibration method, including the one presented here. We want to test the calibration method independent of a particular wireless transceiver technology. Thus in order to have measurements with errors in the centimeters range we used common construction tools, such as tape measures, rulers, plumb-blob, to carefully measure the coordinates of each landmark location in the camera coordinate

system and the distances between the reference camera and the landmark. Using a laser range finder we estimated that the errors incurred using those construction tools are in the order of $\pm$ 2 or 3 cm, which are in the same range the estimation errors one has when using UWB technology (Dardari et al., 2009).

Unless a global localization method is used, such as using GPS devices, the actual coordinates at each location of a roaming robot is usually not known. In our mathematical model (Section 3.1.2), the variables assumed to be known are the vectors between the landmarks' locations in the reference camera coordinate system and the image coordinates of each landmark location. In our experiments, the measurements of the landmarks' coordinates are not used directly in the calculations. These measurements are used to calculate the vectors between the landmarks. When this calibration method is used in a mobile robotic network, these vectors can be obtained from the robots' navigation system. It should be noted that with current GPS technology localization errors in the order of centimeters is not possible unless additional hardware is included.

The CMUcam3 used for the experiments was mounted in a regular office environment. A wood frame was built to support the camera in a way that the Z axis (principle axis) is in the horizontal direction. Fig. 5 shows the front and top view of the CMUcam3 and the mounting structure.

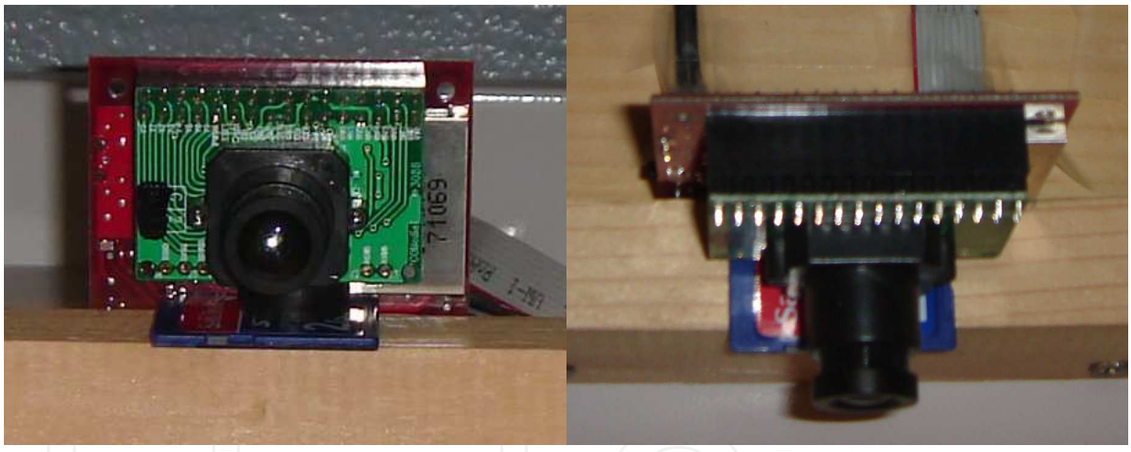

Front view Top view

Fig. 5. The CMUcam3.

The active landmark was built using the metal structure parts from the VEX robotics design system (Cass, 2006) and LEGO bricks with holes. With the wireless communication capabilities, the robots can turn on and off the LEDs whenever needed to form visible landmarks. Fig. 6 shows the pictures of the robot frame where the LEDs are in ON and OFF state.

The metal frame with the active landmark was placed in different locations in the room. For our experiment twelve locations were chosen so that the landmarks were spread out in the image plane. A newly developed efficient blob finding algorithm (Liu & Pomalaza-Ráez, 2010b) was used to automatically find the landmark anywhere in a scene and then calculate the centroid of the landmark. Fig. 7 shows the picture of one of the landmark locations and the output from the blob finding algorithm.

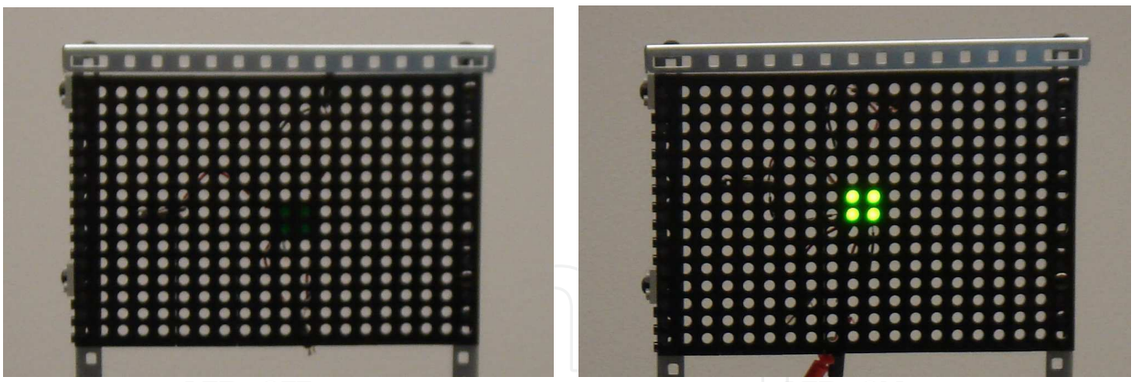

LEDs OFF LEDs ON

Fig. 6. Active landmarks.

The measurements of the landmarks in the twelve locations are shown in Table 1. A_x, A_y, and A_z are the coordinates in the camera coordinate system. L is the magnitude of the $\boldsymbol{A}$ vector, a_x and a_y are the image coordinates. To make full use of the measurements $n(n-1)/2$ equations can be generated from the n locations as shown in Fig. 3.

Landmark OFF Landmark ON Centroid of the landmark

Fig. 7. Pre- and post-processed images by the CMUcam3.

	A_x (cm)	A_y (cm)	A_z (cm)	L (cm)	a_x (pixels)	a_y (pixels)
1	-3.4	-41.0	184.5	188.0	166	45
2	-61.0	-41.0	189.0	199.0	47	49
3	-21.0	-41.0	230.0	232.0	145	63
4	-66.0	-41.0	229.0	239.0	61	65
5	-10.0	2.0	176.6	176.6	153	149
6	-74.0	2.0	177.8	189.6	11	147
7	-12.0	2.0	224.0	224.0	151	148
8	-67.0	2.0	228.4	235.2	56	147
9	33.0	-46.0	264.4	271.5	228	70
10	29.0	-3.0	287.0	287.7	218	143
11	50.0	31.5	272.5	281.3	251	197
12	-66.0	36.5	223.5	232.7	60	215

Table 1. Measurements.

Thus the twelve points listed in Table 1 can be used to generate a maximum of (12x11)/2=66 equations. In order to compare the results of the calibration model using different numbers of measurements and their corresponding equations, our calculation used 5 to 12 locations that generate 10 to 66 equations. The calculation results are shown in Table 2.
In the datasheet of the CMUcam3, the range of values for the focal length f is (2.8~4.9mm). With the value of m_x and m_y, we can calculate the range for α to be (311.1~544.4) and for β to be (341.5~597.6). It is difficult to know what the exact value of f is, thus the exact values of α and β cannot be known either. However, the ratio of α/β is known and is equal to m_x/m_y (0.91). The relative errors of the estimation of the intrinsic parameters are shown in Fig. 8. The estimation results show that the estimates of the parameters converge to the correct values as more measurements are used.

No. of data points	Image sets used	α	β	u_0	v_0	α/β
10	1 → 5	391.9	440.0	174.6	143.0	0.89
15	1 → 6	392.6	368.1	175.4	128.3	1.07
21	1 → 7	394.0	386.1	175.5	132.0	1.02
28	1 → 8	393.3	371.2	175.3	130.0	1.06
36	1 → 9	395.0	452.6	175.2	145.3	0.87
45	1 →10	396.0	451.0	175.0	145.4	0.88
55	1 →11	397.5	442.0	175.3	144.4	0.90
66	1 →12	399.7	442.5	176.0	144.0	0.90
Intrinsic parameters				176	143	0.91

Table 2. Calibration results.

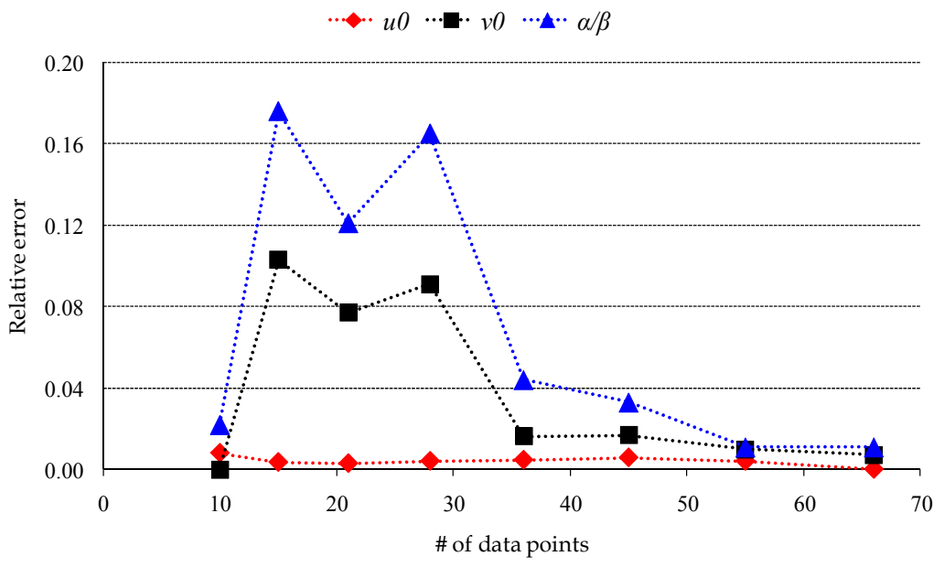

Fig. 8. Relative errors when computing the camera intrinsic parameters.

More than one landmark suited robot can be used in this model to collect a larger number of samples without increasing the amount of time needed to have enough measurements. The mathematical model itself is unchanged when using multiple robots. One advantage when using two or more robots is that it is possible to estimate the distance between the various locations by just using the measurements of the strength of the wireless communication signals between the robots. This type of estimation is possible if for each pair of location points one can position a robot at each point. A minimum of two mobile robots is then needed to obtain a set of measurements.

7. Future developments

The active self-landmarking described in this chapter requires energy efficient LED devices. Currently there is a lot of interest in organic LEDs (OLED). They can be fabricated on flexible substrates which can better fit a variety of robot shapes. Once OLEDs are at the stage to be used in outdoors they will be good candidates for active-landmarking applications. UWB transceivers have shown to provide distances estimation accuracy with errors less than 5 cm which makes them ideal for many localization applications. There are only few commercial suppliers of UWB devices for particular applications. Research in UWB antennas and signal processing is still an active area. It is expected that in the coming years UWB transceivers suitable for robotics applications will be readily available.

To further our research in autonomous mobile robots we are currently building two platforms, equipped with cameras and wireless communication capabilities. Unlike other robot platforms which usually have a computer on board, each of these robots has a single-board RIO (reconfiguration I/O) based microcontroller. The wireless router integrated with the robot is Linksys WRT160N, which is 802.11b/g/n compatible. The choice of cameras is still not finalized. Our goal is to have real-time mobile robot platforms. In order to fully control the image grabbing and transmitting process, we have decided to build the vision system on our own by integrating a FIFO memory with the camera.

8. Conclusion

In this chapter, a new method for fast camera calibration is presented and tested using a smart-camera, the CMUcam3 camera. This method can be easily implemented in a camera-equipped wireless mobile robotic network, where the robots use each other as landmarks. The distances between the robots can be estimated using the wireless signals supported by standard communication protocols. Active landmarks made of LEDs are proposed. The LEDs can be turned on and off through wireless communications commands. One of the limitations of this method is that it relies on the ranging accuracy of the wireless signals measurements. Signals using the protocol 802.15.4 will give errors in the order of meters (not acceptable for calibration tasks). UWB technology, which has errors in the order of centimetres, is more appropriate for this type of application.

9. Acknowledgment

The authors would like to thank the Indiana Space Consortium for their support of the work presented in this chapter.

10. References

Atiya, S. & Hager, G. D.(2000) . Real-time vision-based robot localization, *IEEE Transactions on Robotics and Automation*, pp. 785-800, Vol. 9, No. 6, ISSN : 1042-296X, Dec 1993 .

Bahillo, A.; Prieto, J.; Mazuelas, S.; Lorenzo, R.; Blas, J. & Fernández, P. (2009). IEEE 802.11 Distance Estimation Based on RTS/CTS Two-Frame Exchange Mechanism. *Proceedings of the 2009 IEEE 69th Vehicular Technology Conference*, pp. 1-5, ISBN: 978-1-4244-2517-4, Barcelona, Spain, April 26-29, 2009

Briggs, A.; Scharstein, D.; Braziunas, D.; Dima, C. & Wall, P. (2000). Mobile Robot Navigation Using Self-Similar Landmarks, *Proceeding of the 2000 IEEE International Conference on Robotics and Automation* (ICRA 2000), pp. 1428-1434, ISBN: 0-7803-5889-9 San Francisco, California, USA, April 24-28, 2000.

Cass, S (2006). Getting Vexed, *IEEE Spectrum*, Vol. 43, No. 5, pp. 68-69, ISSN: 0018-9235, May 2006.

Dardari, D.; Conti, A.; Ferner, U.; Giorgetti, A. & Win (2009). Ranging With Ultrawide Bandwidth Signals in Multipath Environments, *Proceedings of the IEEE*, Vol. 97, No. 2, pp. 404-426, February 2009

Falsi, C.; Dardari, D.; Mucchi, L. & Win, M. (2006). Time of Arrival Estimation for UWB Localizers in Realistic Environments, *EURASIP Journal on Applied Signal Processing*, Vol. 2006, 01 January, pp. 1-13, ISSN:1110-8657.

Faugeras, O.; Quan, L. & Strum, P. (2000). Self-calibration of a 1D projective camera and its application to the self-calibration of a 2D projective camera, *IEEE Transactions on Pattern Analysis and Machine Intelligence*, Vol. 22, No. 10, pp. 1179-1185, ISSN: 0162-8828, October 2000

Hoover, A. & Olsen, B. (2000). Sensor network perception for mobile robotics, *Proceedings of the 2000 IEEE International Conference on Robotics and Automation (ICRA 2000)*, Vol. 1, pp. 342-347, ISBN: 0-7803-5886-4, San Francisco, California, USA, April 24-28, 2000

Kurazume, R.; Hirose, S.; Nagata, S. & Sahida, N. (1996). Study on Cooperative Positioning System: Basic Principle and Measurement Experiment, *Proceedings of the 1996 IEEE International Conference on Robotics and Automation*, Vol. 2, pp. 1421-1426, ISBN: 0-7803-2988-0, Minneapolis, Minnesota, USA, April 22-28, 1996

Liang, Q.; Samn, S. & Cheng, X. (2008). UWB Radar Sensor Networks for Sense-through-Foliage Target Detection, *Proceedings of the 2008 IEEE International Conference on Communications*, pp. 2228-2232, ISBN: 978-1-4244-2075-9, Beijing, China, May 19-23, 2008

Lin, C. & Tummala, R. (1997). Mobile Robot Navigation Using Artificial Landmarks, *Journal of Robotics Systems*, Vol. 14, pp. 93-106, February 1997

Liu, Y.; Hoover, A. & Walker, I. (2000). Sensor Network Based Workcell for Industrial Robots, *Proceedings of the IEEE/RSJ International Conference on Intelligent Robots and Systems*, pp. 1434-1439, ISBN: 0-7803-6348-5, Hawaii, USA, October 2001.

Liu, Y. & Pomalaza-Ráez, C. (2010a). Application of Active Self-Landmarking to Camera Calibration, *Proceedings of the International Conference on Machine Vision (ICMV 2010)*, ISBN: 978-1-4244-8888-9, Hong Kong, China, December 28-30, 2010

Liu, Y. & Pomalaza-Ráez, C. (2010b). On-Chip Body Posture Detection for Medical Care Applications Using Low-Cost CMOS Cameras, *Journal of Integrated Computer-Aided Engineering*, Vol. 17, No. 1. pp. 3-13, ISBN: 1069-2509, 2010

Luthy, K.; Grant, E. & Henderson, T. (2007). Leveraging RSSI for Robotic Repair of Disconnected Wireless Sensor Networks, *Proceedings of the 2007 IEEE International*

Conference in Robotics and Automation (ICRA), pp. 3659-3664, ISBN: 1-4244-0601-3, Roma, Italy, April, 2007

Needham, J. (1986). *Science and Civilization in China: Volume 4, Physics and Physical Technology, Part 1, Physics*, Taipei, Caves Books Ltd

Rinner, B.; Winkler, T.; Schriebl, W.; Quaritsch, M. & Wolf, W. (2008). The Evolution from Single to Pervasive Smart Cameras, *Proceedings of the ACM/IEEE International Conference on Distributed Smart Cameras (ICDSC-08)*, pp. 1-10, ISBN: 978-1-4244-2664-5, Stanford University, California, USA, September 7-11, 2008

Rinner, B. & Wolf, W. (2008). An Introduction to Distributed Smart Cameras, *Proceedings of the IEEE*, Vol. 96, pp. 1565-1575, ISSN: 0018-9219, October 2008

Shimizu, Y. & Sanada, Y. (2003). Accuracy of Relative Distance Measurement with Ultra Wideband System, *Proceedings of 2003 IEEE Conference on Ultra Wideband Systems and Technologies*, pp. 374-378, ISBN: 0-7803-8187-4, Reston, Virginia, USA, November 16-19, 2003

Steck, S. & Mallot, H. (2000). The Role of Global and Local Landmarks in Virtual Environment Navigation, *Presence: Teleoperators and Virtual Environments*, Vol. 9, pp. 69-83, ISSN: 1054-7460, February 2000

Schwarzer, S.; Vossiek, M.; Pichler, M. & Stelzer, A. (2008). Precise Distance Measurement with IEEE 802.15.4 (ZigBee) Devices, *Proceedings of the 2008 IEEE Radio and Wireless Symposium*, pp. 779-782, ISBN: 1-4244-1463-6, Orlando, Florida, USA, January 22-24, 2008

Tsai, R. (1987). A Versatile Camera Calibration Technique for 3D Machine Vision, *IEEE Journal of Robotics & Automation*, Vol. 3, No. 4, pp.323-344, ISSN: 0882-4967, August 1987.

Vlasak, A. (2006). The Relative Importance of Global and Local Landmarks in Navigation by Columbian Ground Squirrels (*Spermophilus Columbianus*), *Journal of Comparative Psychology*, Vol. 120, pp. 131-138

Whitehouse, K.; Karlof, C.; Woo, F. Jiang, F. & Culler, D. (2005). The Effects of Ranging Noise on Multihop Localization: An Empirical Study, *Proceedings of the 4th International Symposium on Information Processing in Sensor Networks*, pp. 73-80, ISBN:0-7803-9202-7, Los Angeles, California, USA, April 25-27, 2005

Wu, F.; Hu, Z. & Zhu, H. (2005). Camera calibration with moving one-dimensional objects, *Pattern Recognition*, Vol. 38, No. 5, pp. 755-765, ISSN: 0031-3203, May 2005.

Yokoya, T.; Hasegawa, T. & Kurazume, R. (2008). Calibration of distributed vision network in unified coordinate system by mobile robots, *Proceedings of the 2008 International Conference on Robotics and Automation*, pp. 1412-1417, ISBN 978-1-4244-1647-9, Pasadena, California, USA, May 19-23, 2008

Yoon, K. & Kweon, I. (2001). Landmark design and real-time landmark tracking for mobile robot localization, *Proceedings of The International Society for Optical Engineering (SPIE)*, Boston, USA, Vol. 4573-21, pp. 219-226, October 29-November 2, 2001

Zetik, R.; Crabbe, S.; Krajnak, J.; Peyerl, P.; Sachs, J. & R. Thomä, R. Detection and localization of persons behind obstacles using M-sequence through-the-wall radar, *Proceeding of the SPIE Defense and Security Symposium*, Vol. 6201, ISBN: 9780819462572, 2006, Orlando, Florida, USA, April 17-21, 2006.

Zhang, Z. (2004). Camera Calibration with One-Dimensional Objects, *IEEE Trans. Pattern Analysis and Machine Intelligence*, 26(7):892-899, 2004.

Zitova, B. & Flusser, J. (1999). Landmark recognition using invariant features, *Pattern Recognition Letters,* Vol. 20, pp. 541-547

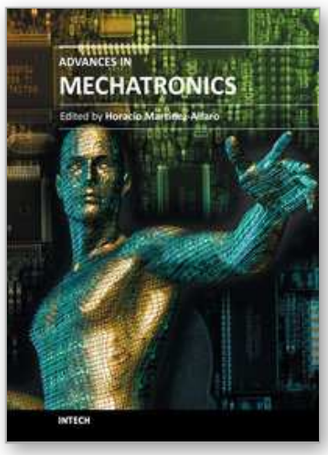

Advances in Mechatronics

Edited by Prof. Horacio Martinez-Alfaro

ISBN 978-953-307-373-6
Hard cover, 300 pages
Publisher InTech
Published online 29, August, 2011
Published in print edition August, 2011

Numerous books have already been published specializing in one of the well known areas that comprise Mechatronics: mechanical engineering, electronic control and systems. The goal of this book is to collect state-of-the-art contributions that discuss recent developments which show a more coherent synergistic integration between the mentioned areas.Â Â The book is divided in three sections. The first section, divided into five chapters, deals with Automatic Control and Artificial Intelligence. The second section discusses Robotics and Vision with six chapters, and the third section considers Other Applications and Theory with two chapters.

How to reference

In order to correctly reference this scholarly work, feel free to copy and paste the following:

Yanfei Liu and Carlos Pomalaza-Ráez (2011). Self-Landmarking for Robotics Applications, Advances in Mechatronics, Prof. Horacio Martinez-Alfaro (Ed.), ISBN: 978-953-307-373-6, InTech, Available from: http://www.intechopen.com/books/advances-in-mechatronics/self-landmarking-for-robotics-applications

INTECH
open science | open minds

InTech Europe
University Campus STeP Ri
Slavka Krautzeka 83/A
51000 Rijeka, Croatia
Phone: +385 (51) 770 447
Fax: +385 (51) 686 166
www.intechopen.com

InTech China
Unit 405, Office Block, Hotel Equatorial Shanghai
No.65, Yan An Road (West), Shanghai, 200040, China
中国上海市延安西路65号上海国际贵都大饭店办公楼405单元
Phone: +86-21-62489820
Fax: +86-21-62489821

© 2011 The Author(s). Licensee IntechOpen. This chapter is distributed under the terms of the Creative Commons Attribution-NonCommercial-ShareAlike-3.0 License, which permits use, distribution and reproduction for non-commercial purposes, provided the original is properly cited and derivative works building on this content are distributed under the same license.

IntechOpen

IntechOpen